Origami-Inspired Shape-Changing Phased Array

D. Elliott Williams[#1], Charles Dorn[*], Sergio Pellegrino[*], Ali Hajimiri[#]
[#]Caltech Holistic Integrated Circuits Lab, Caltech, Pasadena, CA 91125, USA
[*]Graduate Aerospace Laboratories, Caltech, Pasadena, CA 91125, USA
[1]elliott@caltech.edu

***Abstract* — *In situ* geometric reconfiguration of a phased array increases the diversity of radiation patterns that can be synthesized by the array. Such shape-changing phased arrays enable new applications by dynamically conforming their shapes to the geometry best suited for a given task. This work presents the design and demonstration of an origami-inspired shape-changing array built out of identical radiating tiles held in place by a mechanical backbone. The array is capable of shifting into planar, spherical, and cylindrical configurations. The benefits of such an array are analyzed by comparing the properties of different geometries and verified with measurements of the first origami-inspired shape-changing phased array.**

***Keywords* — phased arrays, origami, adaptive arrays, aperture, patch antennas, integrated circuits.**

I. Introduction

The versatility of traditional phased arrays has enabled a wide range of applications by allowing the electronic reconfiguration of an RF transducer's radiation pattern. However, the achievable radiation patterns are still limited by the array geometry; the maximum gain is limited by the volume [1], the grating lobes are limited by the element spacing, and the steering range is limited by the orientations of the element apertures. Phased arrays conformal to different geometries, such as planar, cylindrical, and spherical, have been extensively explored. Planar arrays have been shown to have a higher broadside gain but a more limited scan range than spherical arrays [2]. Much of the exploration of phased arrays has assumed that the geometry is fixed, limiting the space of achievable radiation patterns. There is thus an opportunity to enhance the capabilities of phased arrays by introducing dynamic geometric reconfigurability into the design space.

The idea of combining origami folding techniques and antennas is not new. There has been much work on origami antennas, that is, single element radiating structures that use origami to achieve a particular goal such as deployability [3] or for adjustable frequency [4], polarization [5], and radiation pattern [6]. In general, these structures are single port devices whose radiation properties are not electronically controllable. While some origami antennas have been embedded into an array, in these cases the array itself is fixed; the shape change occurs within an element and not across the array.

Exploration of mechanical reconfigurability across an array has been much more limited. Origami has been used to design frequency-selective surfaces [7]; mechanically reconfigurable arrays of passive elements that can change shape in order to alter their interactions with incident electromagnetic fields. They are essentially reconfigurable RF metamaterials and show promise for novel antenna designs and applications. However, the lack of ports on the elements precludes these surfaces from being used as antennas. In addition, reconfigurable patch arrays with at most four elements have been explored [8]. However, these arrays are driven with a single feed and are not capable of beam steering like a phased array, and thus behave like a single antenna element. The full opportunity presented by geometric reconfigurable arrays has not been explored.

To the authors' best knowledge, this work presents the first origami-inspired shape-changing phased array. First, theory on the benefits of geometric reconfigurability is explored. Then the design of a 3-by-5 element shape-changing phased array is presented. The array can morph into a planar configuration for maximum gain, a spherical configuration for maximum steering range, and a cylindrical configuration for both large gain and steering range in one direction. Finally, measurements of the array verify the presented theory and demonstrate the advantages of shape-changing phased arrays.

II. Gain Properties of Conformal Arrays

A. Relative Gain of Planar and Spherical Arrays

The relationship between the size of an antenna and its maximum gain has been well studied [1]. For electrically large arrays, the maximum achievable gain of the array is proportional to its cross-sectional area. When viewed from broadside, a planar antenna array has a cross-sectional area $A_{cross,plane} = A_{plane}$ and the maximum possible gain is

$$G_{max,plane} = 4\pi \frac{A_{plane}}{\lambda^2}. \quad (1)$$

Suppose the antennas of this array are arranged on the surface of a sphere of radius R, so that they form a spherical cap with the same surface area as the planar array[1]. A cap on a sphere can be parameterized by the arc formed by azimuth angle $0 \leq \phi \leq 2\pi$ at a particular zenith angle θ_c, with an area

$$A_{cap} = \int_0^{\theta_c} \int_0^{2\pi} R^2 \sin(\theta) d\phi d\theta = 2\pi R^2 \big(1 - \cos(\theta_c)\big). \quad (2)$$

Equating this to the planar area A_{plane} gives θ_c:

$$\theta_c = \arccos\left[1 - \frac{A_{plane}}{2\pi R^2}\right]. \quad (3)$$

For an array area smaller than a hemisphere[2], the entire

[1]Note that the planar array cannot be exactly replicated on the surface of the sphere because the change in Gaussian curvature necessitates a change in element spacing. Thus we choose to form a spherical cap with the same surface area in order to simplify the analysis.

[2]$A_{plane} \leq 2\pi R^2$

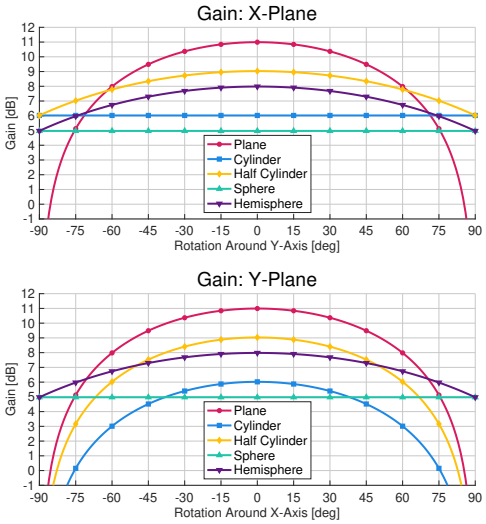

Fig. 1. Theoretical effect of rotation around the $x-$ and $y-$ axes on the gain of an array in various geometric configurations with identical surface area λ^2. The cylinders are oriented along the $x-$ axis.

array is visible to a distant observer at $\theta = 0$. The (visible) cross-sectional area of the array is calculated from the projection of the cap onto a plane. The radius of this circle, r_{proj}, is calculated by the spherical-to-cylindrical conversion:

$$r_{proj} = R\sin(\theta_c) = R\sqrt{1 - \left[1 - \frac{A_{plane}}{2\pi R^2}\right]^2}. \quad (4)$$

Thus the cross-sectional area is

$$A_{cross,sph} = A_{plane}\left[1 - \frac{A_{plane}}{4\pi R^2}\right] \quad (5)$$

which quantifies the visible array area reduction when mapped onto a sphere. For a large sphere $R^2 \gg A_{plane}$, the curvature is negligible and the cross-sectional area is unaffected. However $A_{cross,sph}$ is cut in half if the array covers an entire hemisphere. For even larger arrays, the additional area falls on the opposite side of the sphere and is occluded and the cross-sectional area reduces to that of a sphere, πR^2. The maximum gain of the array mapped to the sphere is thus

$$G_{max,sphere} = G_{max,plane} - \left[\frac{A_{plane}}{\lambda R}\right]^2. \quad (6)$$

B. Effect of Rotation on Gain

Figure 1 demonstrates how the gain of different geometric shapes changes as the object is rotated about the x- and y-axes. As in section II-A, each shape has been normalized to have the same surface area. The cylinder and half cylinder are both orientated along the x-axis. The plane has the largest broadside gain and highest sensitivity to rotation. The sphere has the lowest broadside gain but is insensitive to rotation. The cylinder is insensitive to rotation in one direction and has a larger broadside gain than the sphere. Both the hemisphere and half cylinder have larger broadside gains than their full counterparts because their entire surface area is observable.

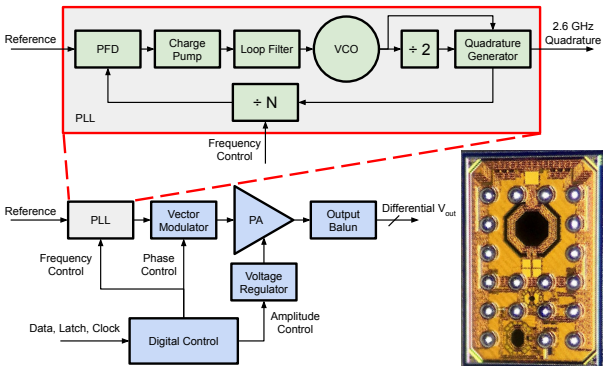

Fig. 2. Antenna driver RFIC block diagram and die photo.

III. Origami-Inspired Phased Array

A. Array Overview

The antenna array consists of 15 identical 6 cm square tiles that are held in a particular shape by an origami inspired metal backbone. Each tile is a self-contained radiating unit consisting of an antenna, a custom antenna driver RFIC, and support electronics. Tiles are attached to the backbone using nylon bolts in order to minimally disturb the antenna. The backbone allows the shape of the array to be easily altered.

The tiles are arranged in series, with the frequency reference, power, and programming signals passed from one tile to the next using flexible cables. The flexible nature of the array makes reliable reference distribution at RF frequencies difficult. Therefore, the output frequency is synthesized from a low frequency reference using a phase locked loop (PLL). In addition, the reference distribution introduces a fixed, but unknown, phase shift between tiles. This phase shift is compensated for using a programmable phase shifter and external calibration. Both the PLL and phase shifter are implemented in a custom RFIC discussed in section III-B.

B. IC Design

A custom 65nm CMOS RFIC drives each antenna element with a 2.6 GHz signal with programmable amplitude and phase. Figure 2 shows a block diagram and die photo of the IC. A type-II PLL with a programmable divider [9] generates quadrature signals at the output frequency $f_{out} = Nf_{ref}$. The vector modulator acts as a phase shifter and a power amplifier (PA) driver by performing a weighted sum of the quadrature signals to set the phase and amplitude of the PA drive, determining its class of operation, linearity, and efficiency. The output stage is a cascode class E/F^{-1} switching PA. A programmable linear regulator controls the supply voltage of the PA, and thus the output power. An on-chip transformer is used as part of the waveform shaping filter, as an impedance transformer, and as a balun to enable the chip to drive both differential and single-ended outputs.

C. Antenna Design

The antenna on each tile is a via-fed linearly polarized patch fabricated on a 120 mil Rogers 6002 substrate. The

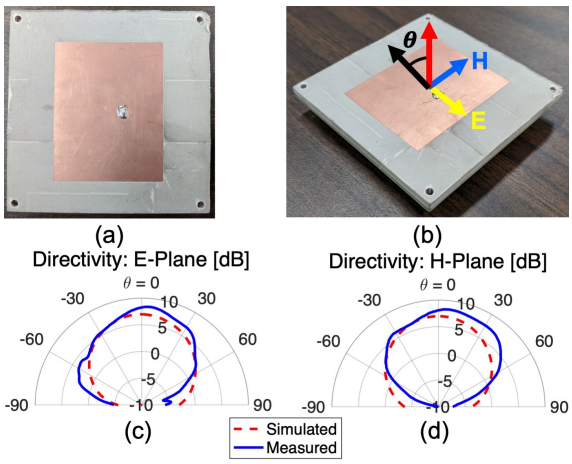

Fig. 3. (a) Tile antenna. (b) Measurement coordinate system. Directivity measurements in (c) E- and (d) H- planes assuming no backside radiation.

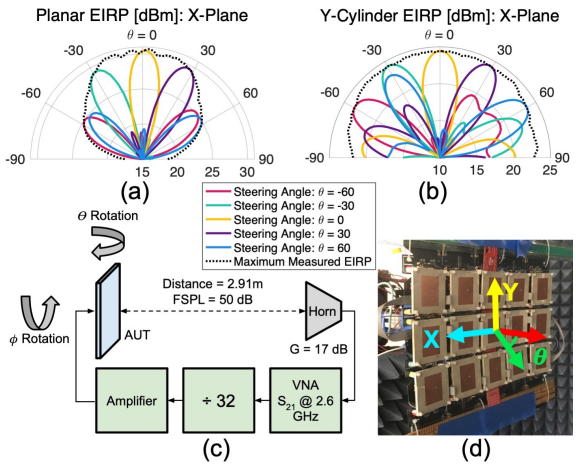

Fig. 4. Subset of x-plane beam patterns and the maximum measured EIRP curves (dotted) for (a) planar and (b) y-cylinder configurations. (c) Diagram of measurement setup. (d) Measurement coordinate system.

length is 32.27 mm and its width is 41.08 mm. The patch ground plane shields the electronics and the metal origami backbone. An L matching network tunes out the feed inductance and matches the antenna to 50Ω at 2.6 GHz. Figure 3 shows the simulated and measured antenna patterns. The measured directivity and HPBW of the antenna is 8.9 dBi and $60.9°$. The simulated efficiency is 98.1%.

D. Mechanical Backbone

The origami-inspired backbone structure allows for reconfiguration of the antenna tiles between spherical, planar, and cylindrical configurations. The geometry consists of a 5-by-5 grid of squares placed on the surface of a sphere of radius 19.6 cm. Adjacent squares are connected by pairs of trapezoids joined by compliant hinges. In the spherical configuration, the trapezoids open into deep valley folds. From the spherical configuration, the valley folds can be closed and the trapezoids brought into contact to achieve planar and cylindrical configurations. In the planar configuration, the antennas are on a 6.75 cm grid, or 0.585λ at 2.6 GHz.

This geometry has 24 kinematic degrees of freedom, so the structure is designed to be bi-stable in the spherical and planar configurations to simplify actuation and facilitate reconfiguration. To achieve bi-stability, torsional springs are embedded on each fold and fold angles are restricted using stops. Specific rest and stop angles of the hinges are selected such that both the spherical and planar configurations are at local strain energy minima. The mountain folds are given a rest angle of zero (fully open) while the valley folds are given a rest angle of π radians (fully folded). The strain energy of the structure is

$$E = \sum_{i \in I_m} \frac{k_m}{2} \theta_i^2 + \sum_{j \in I_v} \frac{k_v}{2} (\theta_j - \pi)^2 \qquad (7)$$

where I_m and I_v index mountain and valley folds and k is the torsional stiffness. The cylindrical configurations can be accessed by tightening a cable between opposite sides of the structure.

To build the structure, compliant hinges have been designed as lamina emergent torsional connections [10] cut by water jet from 0.025 inch thick spring steel. Since the plates and stops are not perfectly rigid and the compliant hinges are not perfect folds, the prototype slightly deviates from ideal planar, spherical, and cylindrical shapes. However, they approximate these shapes closely enough with the aid of external supports to demonstrate the advantages of a reconfigurable array.

IV. Measurements

A. Measurement Setup

Figure 4 (c) shows a diagram of the measurement setup. A vector network analyzer is set to measure S_{21} at 2.6 GHz. A pair of frequency dividers (total division ratio of 32) convert the 2.6 GHz output of the vector network analyzer (VNA) to a 81.25 MHz reference signal. A microwave amplifier buffers the reference signal and supplies it to the antenna under test (AUT). Each tile within the array up-converts the reference back to 2.6 GHz, adjusts the phase, and radiates a fixed power. The combined radiated field is measured by a horn antenna located 2.91 meters from the AUT and connected to the VNA. This distance is larger than the Fraunhofer distance of every measured array configuration. The measured S_{21} is converted to EIRP using a fixed calibration factor. This calibration factor is calculated by measuring a fixed radiation pattern with both the VNA and a power meter and comparing the results.

To measure the radiation pattern, the AUT is mounted horizontally on a far-field scanner and rotated by an angle θ around the y-axis as shown in Figure 4 (d). To steer a beam to a given angle, the AUT is rotated in the opposite direction and the power received by the horn antenna is maximized by using an optimization algorithm to adjust the element phases.

B. Results

A beam is steered in $5°$ increments from $-90°$ to $90°$ in the x-plane and in the y-plane for each configuration shown in Figure 5. An x- or y-plane cut of the beam is

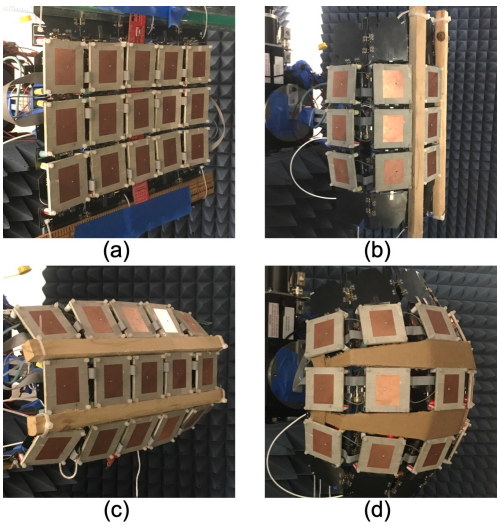

Fig. 5. 3-by-5 tile origami-inspired shape-changing phased array in (a) planar, (b) y-cylinder, (c) x-cylinder, and (d) spherical configurations.

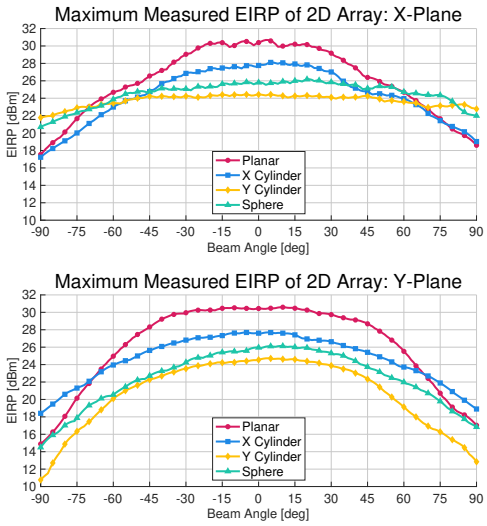

Fig. 6. Maximum measured EIRP as a beam is steered in the x- and y- planes for the 3-by-5 tile array in different geometric configurations.

then measured, depending on which plane the beam is steered in. EIRP patterns of beams steered in the x-plane for the planar and y-cylinder configurations are shown in Figure 4 (a) and (b). These patterns represent only a subset of the 296 measured beam patterns. Because each of these individual patterns contains the maximum achievable EIRP in the steering direction, the maximum of the measured patterns in a plane approximates the maximum achievable EIRP in that plane.

Figure 6 shows the maximum measured EIRP of a beam steered along the x- and y- planes for each configuration. The measured curves follow the trends expected given the theory presented in section II. In particular, shapes with curvature in a given plane exhibit lower maximum EIRP at broadside but less angular sensitivity in that plane than their straight counterparts.

Figure 6 shows some non-idealities that are important to address. Due to the asymmetry inherent in a rectangular 3-by-5 array, each configuration is longer in the x-plane than in the y-plane. Therefore, there is a larger reduction in broadside cross-sectional area and a larger increase in angular coverage due to curvature in the x-plane than in the y-plane. This results in the x-cylinder having a larger maximum broadside EIRP than the y-cylinder. In addition, the x-cylinder has a higher angular sensitivity in the y-plane than the y-cylinder has in the x-plane. It is expected that the two geometries would exhibit identical maximum broadside EIRP and complimentary angular sensitivities in the case of a square array.

As can be seen in Figure 5, the element spacing, and thus the total surface area, is larger in the spherical configuration due to the change in Gaussian curvature. This increase in total area partially compensates for the loss in broadside cross-sectional area due to curvature, making the spherical maximum broadside EIRP higher than the y-cylinder but lower than the planar or x-cylinder configurations. This partial area compensation comes at the cost of increased grating lobes. Finally, the sphere exhibits higher angular sensitivity in the y-plane than in the x-plane due to the rectangular asymmetry.

V. Conclusion

This paper presents the design of a shape-changing phased array operating at 2.6 GHz. The array can morph into planar, cylindrical, and spherical configurations. Measurements of the array show that the planar configuration has a higher maximum EIRP at broadside, but a smaller steering range, than the curved configurations. The reconfigurable nature of the array allows it adapt itself to the geometry best suited for a given application.

Acknowledgment

The authors thank Rogers Corp. for providing substrate materials and R. Lang, B. Abiri, D. Hodge, and Y. Li for their help. This work was supported in part by the MURI Grant FA9550-16-1-0566 via AFOSR.

References

[1] P.-S. Kildal, *et al.*, "Degrees of freedom and maximum directivity of antennas: A bound on maximum directivity of nonsuperreactive antennas," *IEEE Ant. Prop. Mag.*, vol. 59, pp. 16–25, Aug. 2017.

[2] R. F. E. Guy, "Spherical coverage from planar, conformal and volumetric arrays," in *IEE Nat. Conf. on Ant. Prop.*, Mar. 1999, pp. 287–290.

[3] J. Costantine, *et al.*, "Uhf deployable helical antennas for cubesats," *IEEE Trans. Ant. Prop.*, vol. 64, pp. 3752–3759, Apr. 2016.

[4] X. Liu, *et al.*, "A design of an origami reconfigurable qha with a foldable reflector," *IEEE Ant. Prop. Mag.*, vol. 59, pp. 78–105, Aug. 2017.

[5] S. Yao and S. V. Georgakopoulos, "Origami segmented helical antenna with switchable sense of polarization," *IEEE Access*, vol. 6, pp. 4528–4536, Feb. 2018.

[6] X. Liu, *et al.*, "Mode reconfigurable bistable spiral antenna based on kresling origami," in *IEEE Int. Symp. on Ant. Prop.*, Jul. 2017, pp. 413–414.

[7] K. Fuchi, *et al.*, "Origami tunable frequency selective surfaces," *IEEE Ant. Wireless Prop. Lett.*, vol. 11, pp. 473–475, Apr. 2012.

[8] S. R. Seiler *et al.*, "An origami inspired circularly-polarized folding patch antenna array," in *IEEE Int. Symp. on Ant. Prop.*, Jul. 2018, pp. 181–182.

[9] C. S. Vaucher, *et al.*, "A family of low-power truly modular programmable dividers in standard 0.35-μm cmos technology," *IEEE J. Solid-State Circuits*, vol. 35, pp. 1039–1045, Jul. 2000.

[10] J. O. Jacobsen, *et al.*, "Lamina emergent torsional (let) joint," *Mechanism and Machine Theory*, vol. 44, pp. 2098–2109, Jul. 2009.